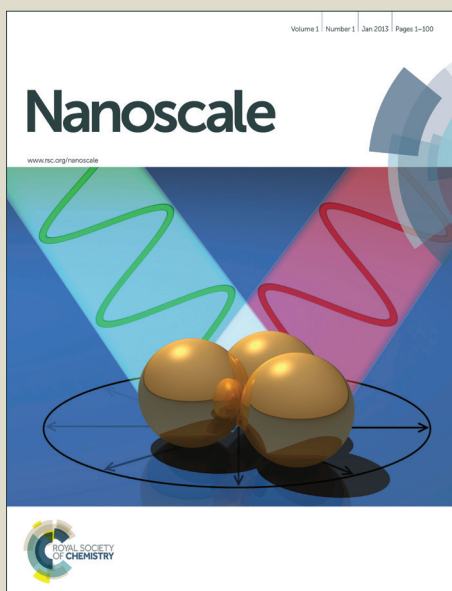


# Nanoscale

Accepted Manuscript



This is an *Accepted Manuscript*, which has been through the Royal Society of Chemistry peer review process and has been accepted for publication.

*Accepted Manuscripts* are published online shortly after acceptance, before technical editing, formatting and proof reading. Using this free service, authors can make their results available to the community, in citable form, before we publish the edited article. We will replace this *Accepted Manuscript* with the edited and formatted *Advance Article* as soon as it is available.

You can find more information about *Accepted Manuscripts* in the [Information for Authors](#).

Please note that technical editing may introduce minor changes to the text and/or graphics, which may alter content. The journal's standard [Terms & Conditions](#) and the [Ethical guidelines](#) still apply. In no event shall the Royal Society of Chemistry be held responsible for any errors or omissions in this *Accepted Manuscript* or any consequences arising from the use of any information it contains.

## COMMUNICATION

## Nanospace-confined formation of flattened Sn sheets in pre-seeded graphenes for lithium ion batteries

Cite this: DOI: 10.1039/x0xx00000x

Zhengjie Li,<sup>a,d,†</sup> Wei Lv,<sup>b,d,†</sup> Chen Zhang,<sup>a,d</sup> Jiwen Qin,<sup>b</sup> Wei Wei,<sup>a,d</sup> Jiao-Jing Shao,<sup>a,d</sup> Da-Wei Wang,<sup>c</sup> Baohua Li,<sup>b</sup> Feiyu Kang,<sup>b</sup> and Quan-Hong Yang<sup>\*a,b,d</sup>

Received 00th January 2014,

Accepted 00th January 2014

DOI: 10.1039/x0xx00000x

www.rsc.org/

**The flattened Sn sheets are prepared from pre-seeded Sn salt in the interlayer nanospaces of a graphene membrane, which is a template to shape Sn crystals and prevent the aggregation. The sandwich structure clamping Sn sheets accommodates the volume change during charge/discharge. We show that the hybrid shows excellent rate performance and cycling stability as an anode for lithium ion batteries.**

Lithium ion batteries (LIBs) are a type of important electrochemical energy storage devices and are considered as the promising power sources for electric vehicles (EVs).<sup>1, 2</sup> However, the energy density of a commercial LIB is somehow unable to meet the colossal energy requirement for EVs. This is partly because of the low capacity of the commercial graphite-based anode materials. Thus, the development of advanced electrode materials with very high energy density is urgently required. Tin (Sn) is one of the most attractive anode materials for LIBs in view of its high theoretical specific capacity (992 mA h g<sup>-1</sup>) and low cost. But an apparent volume change (~250%) that occurs during the charge/discharge process results in poor cyclic stability and power capability, making it hard to be used practically in a commercial battery.<sup>3</sup> Various nanostructures have been designed to solve these problems, but the complicated preparations together with limited performance improvements hinder them from going further into a practical application.<sup>4-7</sup> Recently, it has been reported that a sheet-like structure of non-carbon materials can greatly improve their cyclic stability and power capability owing to the shortened Li ion diffusion paths, larger effective reaction area and smaller volume expansion.<sup>8-11</sup> However, due to the low melting point of Sn, it is hard to obtain a sheet-like structure by a normal preparation process unless one uses an ultrafast cooling process from high temperature that is difficult to be realized in a large scale.<sup>12, 13</sup>

Graphene, as a novel thin and flexible planar carbon material, is widely used to improve the electrochemical performance of various noncarbon electrode materials as a conducting filler or

buffer structure<sup>14-18</sup> and our previous efforts have also demonstrated the effectiveness of graphene as “the most flexible and thinnest carbon additive” to improve the performance of noncarbon electrodes.<sup>19-23</sup> Thus far, the structural characteristics of graphene-based materials, like the 2D nanospace in a graphene membrane, has been rarely fulfilled to template or shape the formation of a noncarbon material since the slit-like nanospace is too narrow to allow foreign components as a precursor in.

In this study, we proposed a pre-seeding technique to prepare sheet-like materials in a graphene membrane. This technique is exclusively for metals or metal oxides with a low melting point like Sn and the 2D confinement effect is fully employed for shaping the formation of flattened Sn sheets (Sn-FSSs) in the interlayer nanospace. The finally obtained graphene/Sn-FSSs hybrid possesses a face-to-face sandwich structure and works as an ideal structure for carbon/noncarbon hybrid anode material, in which a good contact of the two components results in good electron and ion transports and accommodates volume changes of Sn in the charge/discharge process. The hybrid materials therefore show a high reversible capacity as well as excellent cycle performance (650 mA h g<sup>-1</sup> at 100 mA g<sup>-1</sup> after 100 cycles), exhibiting great potential as an anode material for high performance LIBs.

Four key steps are contained in the proposed strategy. Firstly, Sn<sup>4+</sup> is pre-seeded onto graphene oxide (GO) sheet in an aqueous solution due to the electrostatic interaction; then with a filtration process, a GO membrane is formed and Sn<sup>4+</sup> is naturally pre-seeded in the formed interlayer nanospace; the following thermal treatment process results in Sn-FSSs, in which 2D nanospace as a template restricts the aggregation of Sn into particles; the last step is important for further optimizing the electrochemical performance of Sn anode, and that is a fast quenching at low temperature, in which Sn sheet is cut into smaller size in both lateral dimension and thickness and rendered a shortened ion transport path and improved rate performance.

The detailed preparation process of the hybrid membrane is illustrated in Fig. 1. A  $\text{SnCl}_4$ /polyvinyl alcohol (PVA) dispersion was slowly added to a GO hydrosol under sonication to form a homogeneous mixture, and in this process, the  $\text{Sn}^{4+}$  is uniformly distributed on the GO surface, ensuring the uniform loading of the finally formed Sn. Such a mixture was then filtered to obtain a  $\text{Sn}^{4+}$  decorated GO membrane with layered

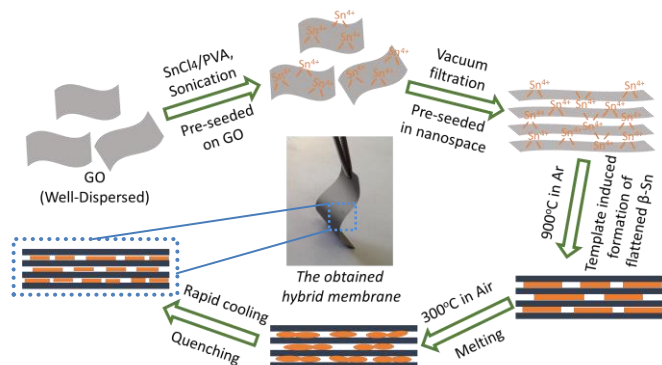


**Fig. 1** Schematic of the formation of the flattened Sn sheets in the interlayer nanospace of graphene membrane, in which  $\text{Sn}^{4+}$  is pre-seeded firstly onto the GO sheet and the formed interlayer nanospace acts as the template shaping the Sn sheet formation and restricting the aggregation of crystal Sn during its growth and quenching process.

structure. The interlayer nanospace in the filtrated membrane acts as a template for the formation of a sheet-like Sn-FSs.  $\text{Sn}^{4+}$ , naturally pre-seeded in the nanospace, is the precursor of Sn sheets. The membrane was treated at  $900\text{ }^\circ\text{C}$  for 2 h under an Ar atmosphere with heating and cooling rates of  $5\text{ }^\circ\text{C min}^{-1}$ , during which the  $\text{Sn}^{4+}$  was reduced to Sn by the carbon.<sup>24</sup> After this treatment, we found that Sn was flattened but with a large size, which can be seen from the cross-sectional scanning electron microscopy (SEM) image shown in Fig. S1(ESI†). Such a membrane is denoted G/Sn-L. In order to further decrease the sheet size and thickness of Sn sheets for a better electrochemical performance, a fierce quenching process rather than a moderate cooling process is favorable for minimizing the sheet size. Thus, the membrane was reheated at  $300\text{ }^\circ\text{C}$  in air (the melting point of Sn is  $\sim 230\text{ }^\circ\text{C}$ ) and then cooled rapidly by immediately immersing it into liquid nitrogen.<sup>25</sup> Considering the high thermal stability of graphene and most of the Sn is protected by the graphene layer,<sup>26</sup> we conducted such heating process in atmosphere to make the following quenching process easy to be operated. The molten Sn forms thin liquid film between the graphene layers, and the following fast quenching process restrains excessive coalescence of liquid Sn into large sheet and the nanospace template helps restrict its movement and aggregation. Thus, smaller and thinner Sn sheet similar to the liquid film state is formed. The final obtained membrane is denoted G/Sn-S. In such a process, the large Sn sheet transforms into thinner and smaller sheet. For comparison, a hybrid without a layered structure was also prepared with the same process as that of G/Sn-L but free from filtration, and the obtained powder sample was denoted G/Sn-F, and an obvious aggregation of Sn is observed in this unfiltered material (Fig. S2, ESI†), indicating the nanospace confinement is important for the formation of sheet-like Sn. The detailed preparation methods for these samples are provided in the ESI†.

The pre-seeding step is crucial for the usage of layer structure as a template for the formation of sheet-like Sn since the

interlayer structure of graphene membrane is too narrow to allow the metal ion precursors in. Such a template shapes the formation of Sn into sheet-like structure and results in Sn sheet/graphene hybrid with sandwich structure simultaneously, which is promising in electrode material for LIB. A photo of the prepared G/Sn-S hybrid membrane is revealed in Fig. 1. Such a membrane is flexible and shows a metallic luster after a thermal treatment.<sup>27, 28</sup> The microstructure of the G/Sn-S hybrid membrane was investigated by SEM and transmission electron microscopy (TEM). Fig. 2a shows the cross-sectional SEM image of the G/Sn-S, from which a layered structure is observed. Compared with G/Sn-L which contains many large Sn sheets (Fig. S1, ESI†), few large Sn sheets are observed in G/Sn-S (Fig. 2a), indicating that the re-heating and quenching process induces the remarkable decrease of both the size and thickness of the Sn-FSs. Note that some particles and large sheets are occasionally observed on the top surface and bottom of the obtained membrane due to the lack of enough confinement in these positions. The Sn-FSs in G/Sn-S possess a lateral size smaller than one micrometer, and are uniformly distributed between the graphene layers, which can be clearly seen in the SEM image of the hybrid membrane surface shown in Fig. 2b. The TEM image (Fig. 2c) clearly shows the Sn-FSs are tightly anchored on the graphene sheets, and with the side length of about 200 nm. It should be mentioned that both the graphene layer and the Sn sheet can be observed clearly by

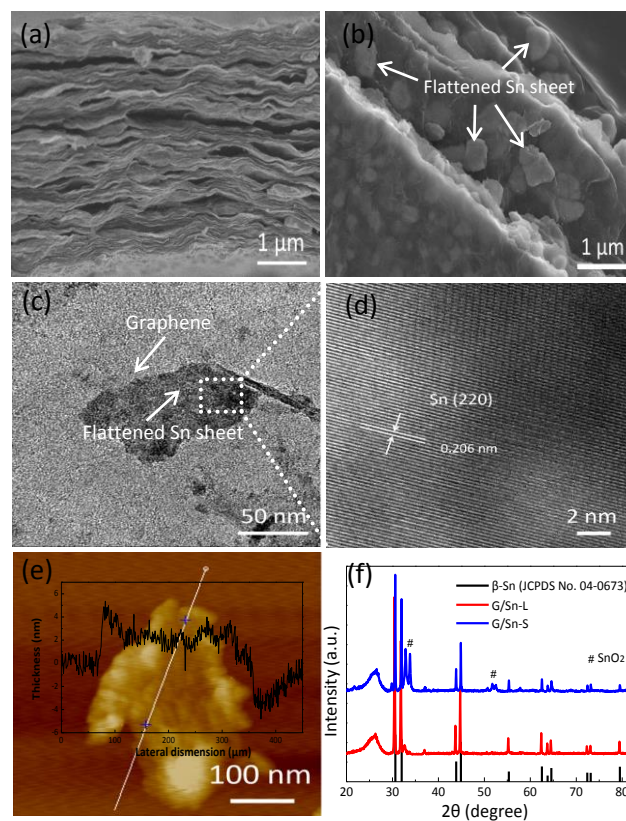


**Fig. 2** (a) Cross-sectional SEM image of the face-to-face stacked layer structure of G/Sn-S; (b) SEM image of a G/Sn-S with a cut fresh wedge surface, from which the uniform flattened Sn sheets can be observed. (c) and (d) TEM images of G/Sn-S. (e) AFM image of G/Sn-S and inset, a profile of a Sn sheet with the line scan showing a thickness of around 10 nm. (f) XRD patterns of G/Sn-L and G/Sn-S.

TEM in one focus length, suggesting the Sn sheet is very thin. A relatively strong interaction exists between the Sn-FS and graphene, which can be proved by the blue shift of the Raman G-band of G/Sn-S compared to that of G/Sn-F (Fig. S3, ESI†). Such an interaction helps the fast electron transfer between the two components during the electrochemical process and ensures the good conductivity of the hybrid membrane (about  $1.6 \Omega/\square$  measured by the four-probe method). Similar interaction can also be observed in the G/Sn-L (Fig. S3, ESI†), indicating the main difference of G/Sn-S and G/Sn-L is the size of Sn sheet. The Sn-FS is crystalline with a lattice spacing of 0.206 nm observed from the high resolution TEM image in Fig. 2d, corresponding to the (220) plane of Sn. The thickness of the Sn-FSs contained in G/Sn-S is further evaluated by atomic force microscopy (AFM) measurements. As shown in Fig. 2e, a Sn-FS separated from G/Sn-S by strong sonication in ethanol and spin-coated on mica substrate has a thickness of about 3–8 nm, suggesting the interlayer nanospace efficiently confines the growth of the Sn-FSs during the thermal treatment and quenching process. As shown in Fig. S4 (ESI†), the interlayer spacing of the adjacent layers of the membrane is about 9–10 nm which is much larger than that of the pure graphene membrane (~0.4 nm as shown by the sharp peaks located at about  $25^\circ$  in the X-ray diffraction (XRD) pattern, Fig. S5, ESI†), suggesting the Sn-FSs are intercalated between the graphene layers and have a thickness of about 7–8 nm, in agreement with the AFM results shown in Fig. 2e. Note that the inner part of the membrane is flat and no rounded particle exists. This further indicates the Sn in the membrane is with a sheet-like structure that is similar to graphene.

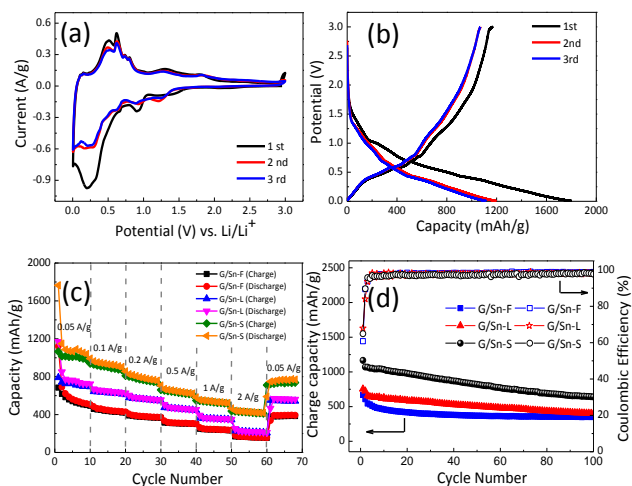


**Fig. 3** (a) CV curves of a G/Sn-S anode at a scanning rate of  $0.1 \text{ mV s}^{-1}$ . (b) Galvanostatic charge/discharge profiles of a G/Sn-S anode at a current density of  $0.1 \text{ A g}^{-1}$ . (c) The rate capability and (d) the cycling stabilities and Coulombic efficiency of the G/Sn-F, G/Sn-L and G/Sn-S with a current density of  $0.1 \text{ A g}^{-1}$ .

XRD patterns shown in Fig. 2f prove the existence of Sn in the hybrid membrane. The main peaks of the G/Sn-L and G/Sn-S are agreement with those of  $\beta$ -Sn (JCPDS No. 04-0673). Some typical peaks of  $\text{SnO}_2$  can also be observed, which may be due to mild oxidation during the reheating process. For the  $\text{Li}^+$  storage process,  $\text{SnO}_2$  possesses a lower specific capacity than Sn and meanwhile, is of very low fraction in the prepared hybrid (indicated by the much lower intensity compared with that of Sn). Therefore,  $\text{SnO}_2$  is not considered in the evaluation

of the specific capacitance of the prepared hybrid, which should have a very limited influence on the real performance of G/Sn-S. The Sn content of the hybrid membrane is about 46 wt% determined by thermogravimetric analysis (TGA) conducted in air (Fig. S6, ESI†). The weak and broadened XRD peak located at about  $25^\circ$  may be derived from the partially overlapped graphene sheets in the hybrid membrane.<sup>29</sup>

The electrochemical performance of the G/Sn-S was evaluated as an anode material for LIBs. Fig. 3a shows the cyclic voltammograms (CV) of the initial 3 cycles of G/Sn-S with a scan rate of  $0.1 \text{ mV s}^{-1}$ . The broad reduction peaks at 0.2–0.7 V are attributed to multistep electrochemical reduction reactions due to the insertion of  $\text{Li}^+$  into Sn to form Li–Sn alloys ( $\text{Li}_x\text{Sn}_y$ ). Four distinct oxidation peaks at 0.4–0.8 V correspond to the delithiation reaction of  $\text{Li}_x\text{Sn}_y$  alloys.<sup>12, 25, 30, 31</sup> The large reduction peak near 0.3 V in the first cycle may be attributed to the formation of a solid-electrolyte interface (SEI) film. No peaks vanish after the first cycle although the cathodic peaks decrease in intensity and shift to the right, indicating the irreversible reactions are greatly suppressed in the first cycle, and this is further supported by the relatively high Coulombic efficiency (~65.0%), which is discussed below. For the second and third cycles, the complete overlap of the curves implies good capacity retention and stability. In agreement with the CV profiles, the first discharge profile shows a steep voltage drop to about 1 V which is followed by a sloping curve down to the cutoff voltage of 0.005 V, delivering a large specific capacity of about  $1795 \text{ mA h g}^{-1}$  (Fig. 3b). The initial charge capacity is found to be  $1166 \text{ mA h g}^{-1}$ , corresponding to a Coulombic efficiency of ~65%, and the Coulombic efficiency increases to about 98% after 5 cycles corresponding to a capacity of about  $1000 \text{ mA h g}^{-1}$  (Fig. 3d). Note that the capacity is calculated based on the total mass of the G/Sn-S. In the second charge/discharge cycle, the G/Sn-S anode still has a large reversible capacity of about  $1071 \text{ mA h g}^{-1}$ . After 50 cycles, the capacity remains about  $800 \text{ mA h g}^{-1}$ , revealing good cycle ability. The advantage of such flattened structure of Sn in electrochemical process can be clearly represented in Fig. 3c, and both G/Sn-L and G/Sn-S show superior capacity performance compared with G/Sn-F under various current densities.

The G/Sn-S shows an apparently higher rate performance than G/Sn-L (Fig. 3c), indicating the smaller sheet size is in favour of fast electrochemical kinetics. The capacity of G/Sn-S still reaches  $440 \text{ mA h g}^{-1}$  when the current density increases to  $2 \text{ A g}^{-1}$ , which is much higher than those of G/Sn-L ( $220 \text{ mA h g}^{-1}$ ) and G/Sn-F ( $160 \text{ mA h g}^{-1}$ ). When the current density is switched back to  $50 \text{ mA g}^{-1}$  after more than 60 cycles, a high discharge capacity of  $774 \text{ mA h g}^{-1}$  is recovered. The high rate capability of G/Sn-S may be attributed to the short ion diffusion/migration length due to the sheet structure of Sn discussed above. In addition, the uniform distribution of Sn-FSs among the graphene layers that is revealed by the SEM observation prevents the tight restacking of graphene layers, providing sufficient ion transport channels. The layered structure and the Sn-FSs accommodate large volume changes during the charging/discharging process, preventing the collapse and pulverization of Sn and resulting in the high capacity, and G/Sn-S also exhibits good cycling stability ( $650 \text{ mA h g}^{-1}$  is still retained after 100 cycles). Such good cyclic ability is derived from the stable “sandwich” layer structure (tightly attached Sn and graphene sheets) and, as shown in Fig. S8 (ESI†), the layered structure (full lithiation state) is well maintained after 100 cycles. Note that the membrane was used

as the electrode directly only for the SEM observation to make the cross-section of such a structure easy to be observed, and such integrated membrane was not used for the electrochemical measurement since the inner part of the membrane with large size is hard to be accessed by the electrolyte, resulting in large polarization. Based on the above discussion, we are confident that the rate performance and cyclic stability of G/Sn-S are among the highest reported so far.<sup>3-5, 25, 31-33</sup> Above result clearly indicates the smaller flattened Sn sheets greatly improve the electrochemical performance of the hybrid, especially for the capacity and rate performance, compared with the hybrid with large Sn size. The Nyquist plots (Fig. S9, ESI†) further prove the advantage of such a structure. The diameter of the semicircle for the G/Sn-S electrode in the high-medium frequency region is much smaller than those of G/Sn-L and G/Sn-F, and thus, G/Sn-S possesses lower contact and charge-transfer impedance, which guarantee the good electrochemical performance.

In summary, the interlayer nanospace in a graphene membrane is developed as a novel template for preparing sheet-like nanostructures, in which pre-seeding precursor before the nanospace formation is a key step for the templated growth of nanostructures. Flattened Sn sheets (Sn-FSs) is a typical example presented in this communication. With Sn<sup>4+</sup> pre-seeded onto the GO sheet, the Sn-FSs are obtained in a graphene membrane after the filtration, heating and quenching processes, and the filtration-formed interlayer nanospace shapes the Sn sheet formation and restricting the aggregation of crystal Sn during its growth and quenching process. The formed graphene/Sn-FSs hybrid membrane shows good performance when used as the anode of a lithium ion battery, which is characterized by high capacity, superior rate performance and long cyclic stability due to the restricted volume expansion and shortened ion diffusion. This study indicates a versatile route to produce sheet-like materials, not exclusively for energy storage applications.

We appreciate support from National Basic Research Program of China (2014CB932403), National Science Foundation of China (Nos. 51372167 and 51302146), Shenzhen Basic Research Project (Nos. JC201104210152A) and China Postdoctoral Science Foundation (2013T60111). We also thank the financial support from Guangdong Province Innovation R&D Team Plan (No. 2009010025).

## Notes and references

<sup>a</sup> Key Laboratory for Green Chemical Technology of Ministry of Education, School of Chemical Engineering and Technology, Tianjin University, Tianjin 300072, China; [qhyangcn@tju.edu.cn](mailto:qhyangcn@tju.edu.cn).

<sup>b</sup> Engineering Laboratory for Functionalized Carbon Materials, Graduate School at Shenzhen, Tsinghua University, Shenzhen 518055, China; [yang.quanhong@sz.tsinghua.edu.cn](mailto:yang.quanhong@sz.tsinghua.edu.cn).

<sup>c</sup> School of Chemical Engineering, The University of New South Wales, Sydney, NSW 2033, Australia.

<sup>d</sup> The Synergistic Innovation Center of Chemistry and Chemical Engineering of Tianjin, Tianjin 300072, China.

† Electronic Supplementary Information (ESI) available: Details of the preparation and characterization of G/Sn-F, G/Sn-L and G/Sn-S. See DOI: 10.1039/b000000x/

‡ These authors are equal main contributors.

1. M. V. Reddy, G. V. S. Rao and B. V. R. Chowdari, *Chem Rev*, 2013, **113**, 5364-5457.
2. S. Xin, Y. G. Guo and L. J. Wan, *Accounts Chem Res*, 2012, **45**, 1759-1769.
3. G. X. Wang, B. Wang, X. L. Wang, J. Park, S. X. Dou, H. Ahn and K. Kim, *J Mater Chem*, 2009, **19**, 8378-8384.

4. S. Z. Liang, X. F. Zhu, P. C. Lian, W. S. Yang and H. H. Wang, *J Solid State Chem*, 2011, **184**, 1400-1404.
5. B. Luo, B. Wang, M. H. Liang, J. Ning, X. L. Li and L. J. Zhi, *Adv Mater*, 2012, **24**, 1405-1409.
6. D. N. Wang, X. F. Li, J. L. Yang, J. J. Wang, D. S. Geng, R. Y. Li, M. Cai, T. K. Sham and X. L. Sun, *Phys Chem Chem Phys*, 2013, **15**, 3535-3542.
7. Y. Q. Zou and Y. Wang, *ACS Nano*, 2011, **5**, 8108-8114.
8. S. Q. Chen and Y. Wang, *J Mater Chem*, 2010, **20**, 9735-9739.
9. K. Chang and W. X. Chen, *Chem Commun*, 2011, **47**, 4252-4254.
10. G. M. Zhou, D. W. Wang, L. C. Yin, N. Li, F. Li and H. M. Cheng, *ACS Nano*, 2012, **6**, 3214-3223.
11. R. H. Wang, C. H. Xu, J. Sun, Y. Q. Liu, L. Gao and C. C. Lin, *Nanoscale*, 2013, **5**, 6960-6967.
12. Y. H. Xu, Q. Liu, Y. J. Zhu, Y. H. Liu, A. Langrock, M. R. Zachariah and C. S. Wang, *Nano Lett*, 2013, **13**, 470-474.
13. B. Luo, B. Wang, X. L. Li, Y. Y. Jia, M. H. Liang and L. J. Zhi, *Adv Mater*, 2012, **24**, 3538-3543.
14. G. M. Zhou, D. W. Wang, F. Li, L. L. Zhang, N. Li, Z. S. Wu, L. Wen, G. Q. Lu and H. M. Cheng, *Chem Mater*, 2010, **22**, 5306-5313.
15. H. L. Wang, H. S. Casalongue, Y. Y. Liang and H. J. Dai, *J Am Chem Soc*, 2010, **132**, 7472-7477.
16. Z. J. Fan, J. Yan, L. J. Zhi, Q. Zhang, T. Wei, J. Feng, M. L. Zhang, W. Z. Qian and F. Wei, *Adv Mater*, 2010, **22**, 3723-3728.
17. J. Yan, Z. J. Fan, W. Sun, G. Q. Ning, T. Wei, Q. Zhang, R. F. Zhang, L. J. Zhi and F. Wei, *Adv Funct Mater*, 2012, **22**, 2632-2641.
18. X. T. Huo, P. Zhu, G. Y. Han and J. J. Xiong, *New Carbon Mater*, 2013, **28**, 414-420.
19. F. Y. Su, C. H. You, Y. B. He, W. Lv, W. Cui, F. M. Jin, B. H. Li, Q. H. Yang and F. Y. Kang, *J Mater Chem*, 2010, **20**, 9644-9650.
20. W. Wei, W. Lv, M. B. Wu, F. Y. Su, Y. B. He, B. H. Li, F. Y. Kang and Q. H. Yang, *Carbon*, 2013, **57**, 530-533.
21. T. T. Xie, W. Lv, W. Wei, Z. J. Li, B. H. Li, F. Y. Kang and Q. H. Yang, *Chem Commun*, 2013, **49**, 10427-10429.
22. W. Lv, F. Sun, D. M. Tang, H. T. Fang, C. Liu, Q. H. Yang and H. M. Cheng, *J Mater Chem*, 2011, **21**, 9014-9019.
23. X. C. Chen, W. Wei, W. Lv, F. Y. Su, Y. B. He, B. H. Li, F. Y. Kang and Q. H. Yang, *Chem Commun*, 2012, **48**, 5904-5906.
24. L. Wang, D. Wang, F. X. Zhang and J. Jin, *Rsc Adv*, 2013, **3**, 1307-1310.
25. L. W. Ji, Z. K. Tan, T. Kuykendall, E. J. An, Y. B. Fu, V. Battaglia and Y. G. Zhang, *Energ Environ Sci*, 2011, **4**, 3611-3616.
26. Z. S. Wu, W. C. Ren, L. B. Gao, J. P. Zhao, Z. P. Chen, B. L. Liu, D. M. Tang, B. Yu, C. B. Jiang and H. M. Cheng, *ACS Nano*, 2009, **3**, 411-417.
27. C. M. Chen, Y. G. Yang, Y. F. Wen, Q. H. Yang and M. Z. Wang, *New Carbon Mater*, 2008, **23**, 345-350.
28. C. M. Chen, J. Q. Huang, Q. Zhang, W. Z. Gong, Q. H. Yang, M. Z. Wang and Y. G. Yang, *Carbon*, 2012, **50**, 659-667.
29. C. Wang, J. Ju, Y. Q. Yang, Y. F. Tang, H. Bi, F. H. Liao, J. H. Lin, Z. J. Shi, F. Q. Huang and R. P. S. Han, *Rsc Adv*, 2013, **3**, 21588-21595.
30. C. D. Wang, Y. Li, Y. S. Chui, Q. H. Wu, X. F. Chen and W. J. Zhang, *Nanoscale*, 2013, **5**, 10599-10604.
31. X. S. Zhou, J. C. Bao, Z. H. Dai and Y. G. Guo, *J Phys Chem C*, 2013, **117**, 25367-25373.
32. Y. H. Xu, J. C. Guo and C. S. Wang, *J Mater Chem*, 2012, **22**, 9562-9567.
33. X. J. Zhu, Y. W. Zhu, S. Murali, M. D. Stoller and R. S. Ruoff, *J Power Sources*, 2011, **196**, 6473-6477.